

Accelerate CNNs from Three Dimensions: A Comprehensive Pruning Framework

Wenxiao Wang^{1,2} Minghao Chen¹ Shuai Zhao³ Long Chen⁴ Jinming Hu¹ Haifeng Liu¹ Deng Cai¹
Xiaofei He¹ Wei Liu²

Abstract

Neural network pruning is one of the most popular methods for model acceleration. Most pruning methods, such as filter-level or layer-level pruning, prune the model along one single dimension (*depth*, *width*, or *resolution*) to meet a computational cost requirement. However, such pruning policy often leads to excessive reduction of that dimension, thus inducing a huge accuracy loss. To alleviate this issue, we argue that pruning should be done along three dimensions comprehensively. For this purpose, our pruning framework formulates pruning as an optimization problem. Specifically, it first fits the relations between the model’s accuracy and *depth/width/resolution* via polynomial regression and then maximizes the polynomial to acquire optimal values for three dimensions. Finally, the model is pruned along three dimensions accordingly. In this framework, since collecting too much data used for the regression is very time-costly, we propose two approaches to lower the cost: (1) specializing the polynomial to ensure an accurate regression even with less data; (2) employing iterative pruning and fine-tuning to collect data faster. Extensive experiments show that our algorithm outperforms state-of-the-art pruning and even NAS-based algorithms.

1. Introduction

To deploy pre-trained deep CNNs (Simonyan & Zisserman, 2015; He et al., 2016; Huang et al., 2017; Tan & Le, 2019) on resource-constrained mobile devices, many methods (Ba & Caruana, 2014; Hinton et al., 2015; Liu et al., 2017; He et al., 2019; Frankle & Carbin, 2019) have been proposed for model acceleration, and neural network pruning is one of the most popular. It prunes redundant components (e.g., filters) of CNNs to meet a computational cost requirement.

Currently, dominant pruning methods fall into three cate-

¹State Key Lab of CAD&CG, Zhejiang University, Hangzhou, China ²Tencent Data Platform, Shenzhen, China ³AIRS, The Chinese University of Hong Kong, Shenzhen, China ⁴Tencent AI Lab, Shenzhen, China. Correspondence to: Deng Cai <deng-cai@gmail.com>.

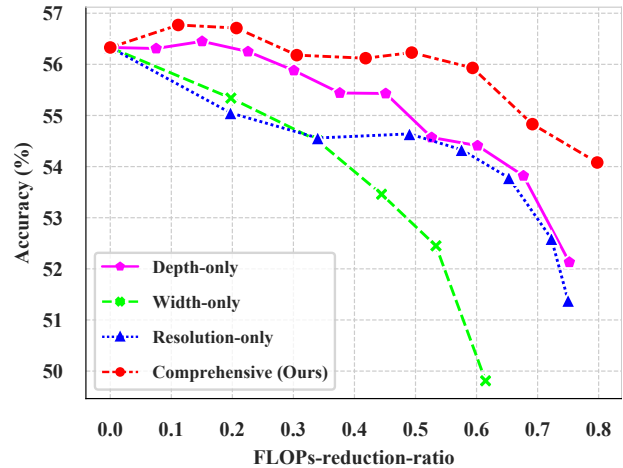


Figure 1. Accuracy of models with different pruning policies on TinyImageNet. The base model is ResNet-56 (FLOPs-reduction-ratio = 0). \mathcal{X} -only means that the model is only pruned along \mathcal{X} dimension, and “comprehensive” means that three dimensions are pruned comprehensively. Larger FLOPs-reduction-ratio indicates a higher acceleration ratio.

gories: (1) **layer-level pruning** (Wang et al., 2019b; Lin et al., 2019), which prunes redundant layers and reduces model’s depth, (2) **filter-level pruning** (Molchanov et al., 2017; He et al., 2019; Wang et al., 2019a; Luo et al., 2019; Kang & Han, 2020), which prunes redundant filters and reduces model’s width, and (3) **image-level pruning**¹ (Howard et al., 2017; Tan & Le, 2019; Han et al., 2020), which resizes images and reduces model’s input resolution. These three kinds of methods respectively focus on one dimension (i.e., depth, width, and image resolution) that affects a model’s computational cost.

Naturally, we raise an important question overlooked by many previous works: given a pre-trained model, which dimension — depth, width, or resolution — should we prune to minimize the model’s accuracy loss? In practice, users empirically choose a redundant dimension, which, however, often leads to a sub-optimal pruned model because of an inappropriate dimension choice. Even worse, excessive pruning of whichever dimension will lead to an unacceptable loss, as shown in Figure 1. Instead, comprehensively

¹Though images are actually resized for acceleration, we will use term “pruning images” for simplicity in the following.

pruning these dimensions yields better results.

In this paper, we propose a framework that prunes three dimensions comprehensively. Instead of directly pruning one dimension to reduce the computational cost, our framework first decides how much of each dimension should be pruned. To this end, we formulate model acceleration as an optimization problem. Precisely, given a pre-trained model and a target computational cost, assuming that the pruned model’s depth, width, and resolution are $d \times 100\%$, $w \times 100\%$, and $r \times 100\%$ of the original model, respectively, we seek the optimal (d, w, r) that maximizes the model’s accuracy a :

$$\max_{d,w,r} a = \mathcal{F}(d, w, r), \text{ s.t. } \mathcal{C}(d, w, r) = \tau, \quad (1)$$

where $\mathcal{F}(d, w, r)$ is a model accuracy predictor (MAP). $\mathcal{C}(d, w, r)$ and τ represent the model’s computational cost and its constraint, respectively. (Tan & Le, 2019) has designed a reasonable expression for $\mathcal{C}(d, w, r)$. However, designing a MAP manually is unachievable as its form can be arbitrarily complicated or even varies with the architecture (e.g., the MAPs for ResNet and MobileNet may be in different forms). Thus, we propose approximating the MAP via polynomial regression because, according to Taylor’s theorem, polynomials can approximate arbitrary continuous functions. Specifically, we can formulate the MAP as a polynomial and collect enough sets of (d, w, r, a) as training data to estimate its parameters. After that, problem (1) can be solved with Lagrange’s multiplier theorem, and the model is pruned in terms of the corresponding (d, w, r) .

The main challenge in this framework is that polynomial regression requires lots of training data (i.e., (d, w, r, a)), while the collection of data is very costly because fetching each set of data means training a new model from scratch. To save time and cost, we improve the framework from two perspectives: (1) A specialized polynomial is proposed whose weight tensor is replaced with its low-rank substitute. The low-rank weight tensor prevents the polynomial from overfitting and ensures an accurate regression even with limited data. Further, as a bonus, the updated MAP owns a more concise form. (2) Given a pre-trained model, we prune and fine-tune the model iteratively to acquire new models and their corresponding (d, w, r, a) , which is much faster than training new models from scratch.

Extensive experiments are conducted to show our preponderance over other pruning algorithms. Further, we compare with some algorithms that balance the size of three dimensions (depth, width, and resolution) from a network architecture search (NAS) perspective. The results also show our advantages over them.

It is worth highlighting our contributions as follows:

- We propose to prune a model from three dimensions comprehensively and determine the optimal values for

these dimensions by solving a regression and an optimization problem.

- To finish the regression process with an acceptable cost, we apply two approaches: (1) specializing a MAP adapting to the limited data scene; (2) using iterative pruning and fine-tuning to collect data faster.
- We do extensive experiments to show that our algorithm performs better than state-of-the-art pruning and even NAS-based model acceleration algorithms.

2. Background and Related Works

Neural Network Pruning: In the early stage, neural network pruning is done at the weight-level (Han et al., 2016; Frankle & Carbin, 2019). However, it needs specific libraries for sparse matrix (e.g., cuSPARSE) to accelerate the inference, while these libraries’ support on mobile devices is limited. Nowadays, the most dominant pruning methods are at the filter-level, layer-level, and image-level, directly reducing the computational cost for all devices. Filter-level pruning (Liu et al., 2017; Li et al., 2017; Molchanov et al., 2017; He et al., 2018; 2019; Wang et al., 2019a; Kang & Han, 2020; Ye et al., 2020; Li et al., 2020; Wang et al., 2020) compresses models by removing unimportant filters in CNNs, layer-level pruning (Wang et al., 2019b) does that by pruning redundant layers, and image-level pruning (Howard et al., 2017) saves computations by using small input images. They all receive great success in pruning CNNs. However, focusing on one dimension solely also restricts their potentials.

Multi-Dimension Pruning: To the best of our knowledge, there are two methods (Wen et al., 2016; Lin et al., 2019) pruning models both at the filter-level and the layer-level. Both of them train models with extra regularization terms and induce sparsity into models. Then filters or layers with much sparsity will be pruned with slight loss. However, the same method cannot be used for balancing image size because images do not contain trainable parameters, and there is no way to induce sparsity into images. In contrast, our framework can balance three dimensions comprehensively, thus yielding better results than the above methods.

Pruning vs. NAS: Pruning and network architecture search (NAS) have the same goal — maximizing a model’s accuracy given a computational cost requirement. However, their settings are different: Pruning shrinks the model from a pre-trained one, utilizing both pre-trained model’s architecture and weights, while NAS searches models from scratch. Therefore, though some algorithms (Tan & Le, 2019; Han et al., 2020) also try to balance the three dimensions (i.e., depth, width, and resolution) of models from a NAS perspective, they cannot be used for pruning directly. Moreover, NAS costs immense amounts of time and resources for searching a new model, which is often computationally prohibitive for a pruning algorithm.

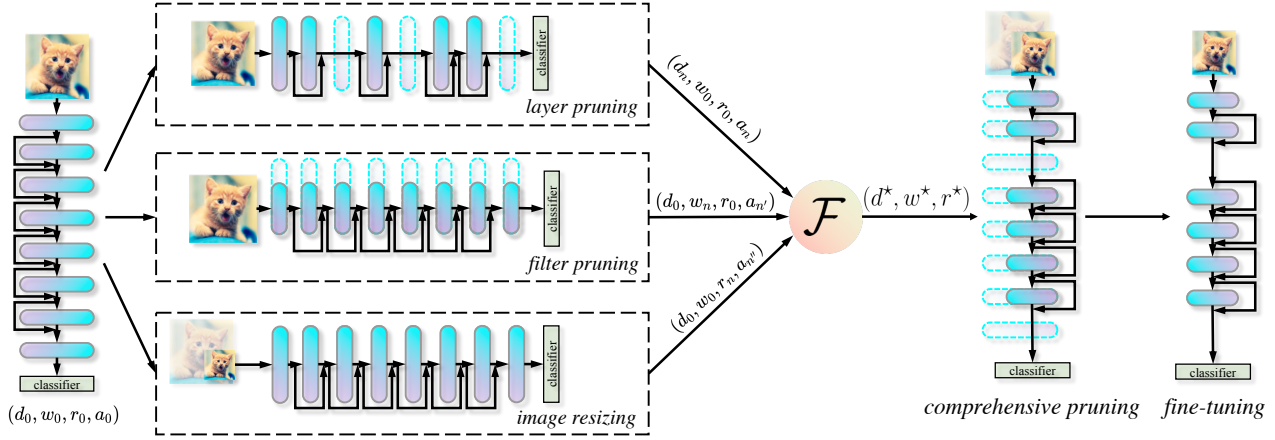


Figure 2. The pipeline of our pruning framework. We first prune the pre-trained model from three dimensions independently, yielding few sets of (d_n, w_n, r_n, a_n) . Then, the data is used to fit our specialized MAP (\mathcal{F}). The optimal (d^*, w^*, r^*) is acquired by optimizing \mathcal{F} under the computational cost constraint. Finally, the model will be pruned comprehensively in terms of (d^*, w^*, r^*) .

3. Proposed Algorithm

3.1. Preliminaries

For a model M , we define $\mathcal{D}(M)$, $\mathcal{W}(M, l)$, and $\mathcal{R}(M)$ as its depth, width, and input resolution. Specifically, $\mathcal{D}(M)$ represents the number of blocks² that M contains; $\mathcal{W}(M, l)$ means the number of filters of a certain layer l in the model M ; and $\mathcal{R}(M)$ is the side length of M 's input image. Further, given a pre-trained model M_0 , we define d_n , w_n , and r_n of a pruned model M_n as:

$$d_n = \frac{\mathcal{D}(M_n)}{\mathcal{D}(M_0)}, w_n = \frac{\mathcal{W}(M_n, l)}{\mathcal{W}(M_0, l)}, r_n = \frac{\mathcal{R}(M_n)}{\mathcal{R}(M_0)}. \quad (2)$$

For filter pruning, following previous works (Luo et al., 2019; He et al., 2019; Lin et al., 2020), we prune all layers with the same ratio, so w_n of a model has no concern with the choice of layer l . Further, for a pruning task, it is easy to know: $d_n, w_n, r_n \in (0, 1]$ and $d_0 = w_0 = r_0 = 1$.

The pipeline of our pruning framework is introduced in Figure 2. Unlike previous works that prune one dimension directly, we first look for a pruning policy (i.e., how much of each dimension should be pruned) that maximizes the model's accuracy in Section 3.2. Then, the process of pruning and fine-tuning the model in terms of the pruning policy is depicted in Section 3.3.

3.2. Model Acceleration as Optimization

3.2.1. FORMULATION

Given a CNN architecture, the model's depth, width, and image resolution are three key aspects that affect both the model's accuracy and its computational cost. Thus, model

acceleration can be formulated as the following problem:

$$d^*, w^*, r^* = \arg \max_{d, w, r} \mathcal{F}(d, w, r; \Lambda) \quad (3)$$

$$s.t. \mathcal{C}(d, w, r) = T \times \mathcal{C}(d_0, w_0, r_0),$$

where $\mathcal{F}(d, w, r; \Lambda)$ is a **model accuracy predictor (MAP)**, which predicts the model's accuracy given (d, w, r) . Λ contains parameters of the MAP. $\mathcal{C}(d, w, r)$ represents the computational cost (e.g., FLOPs) of a model. $T \in (0, 1)$ represents that the pruned model's computational cost is T of the original model. Problem (3) can be solved with the Lagrange's multiplier theorem once $\mathcal{F}(d, w, r)$ and $\mathcal{C}(d, w, r)$ are known. Following (Tan & Le, 2019) in which a model's computational cost is proportional to d, w^2 , and r^2 , we redefine $\mathcal{C}(d, w, r)$ as the following:

$$\mathcal{C}(d, w, r) = dw^2r^2. \quad (4)$$

However, designing a MAP manually is unachievable as its form can be arbitrarily complicated, and different architectures may own different forms. An intuitive idea is resorting to polynomial regression because, according to Taylor's theorem, any continuous function can be approximated with polynomials. Specifically, we can train N models with different (d, w, r) , attaining their accuracy a , and fit the MAP with a polynomial by using these data, i.e., $(d_n, w_n, r_n, a_n), n \in [1, N]$. However, the regression process requires hundreds of sets of data (d_n, w_n, r_n, a_n) for attaining an accurate regression, while fetching each set of data means training a new model from scratch, which is very resource-inefficient and time-consuming. To alleviate the problem, on the one hand, we specialize a MAP that ensures an accurate regression even with few sets of (d, w, r, a) in Section 3.2.2. On the other hand, we accelerate acquiring each set of (d, w, r, a) by utilizing iterative pruning and fine-tuning in Section 3.2.3.

²E.g., Conv-BN-Relu blocks and residual blocks.

3.2.2. SPECIALIZED MAP

The polynomial-based MAP can be represented as:

$$\mathcal{F}(d, w, r; \Lambda) = \sum_{i,j,k=0}^{\mathcal{K}} \lambda_{ijk} d^i w^j r^k, \quad (5)$$

where $\Lambda \in \mathbb{R}^{\mathcal{K} \times \mathcal{K} \times \mathcal{K}}$ is a tensor, and all λ_{ijk} are its elements³. Without any constraint on Λ , the polynomial can be highly flexible and expressive. However, high flexibility also makes it easy to overfit (Bishop, 2006), especially when training data (i.e., (d, w, r, a)) is scarce. To avoid overfitting and ensure an accurate regression with limited data, a relatively simple MAP with less flexibility and expressiveness is required. We achieve this by restricting the rank⁴ of Λ during the regression process, i.e., Λ in the MAP is replaced with its low-rank substitute. Formally, for Λ of rank $\tilde{\mathcal{R}}$, its \mathcal{R} -rank substitute ($\mathcal{R} < \tilde{\mathcal{R}}$) and elements are defined as (Kolda & Bader, 2009):

$$\Lambda \approx \sum_{q=1}^{\mathcal{R}} \vec{s}_q \otimes \vec{u}_q \otimes \vec{v}_q, \quad \lambda_{ijk} \approx \sum_{q=1}^{\mathcal{R}} s_{qi} u_{qj} v_{qk}, \quad (6)$$

where \otimes represents outer product, and $\vec{s}_q, \vec{u}_q, \vec{v}_q \in \mathbb{R}^{\mathcal{K}}$ represent \mathcal{K} -dimensional vectors, e.g., $\vec{s}_q = [s_{q1}, s_{q2}, \dots, s_{q\mathcal{K}}]^T$. Then, replacing λ_{ijk} in Eq. (5) yields:

$$\begin{aligned} \mathcal{F}(d, w, r; \Lambda) &\approx \sum_{i,j,k=0}^{\mathcal{K}} \sum_{q=1}^{\mathcal{R}} s_{qi} u_{qj} v_{qk} d^i w^j r^k \\ &= \sum_{q=1}^{\mathcal{R}} \sum_{i,j,k=0}^{\mathcal{K}} (s_{qi} d^i) (u_{qj} w^j) (v_{qk} r^k) \\ &= \sum_{q=1}^{\mathcal{R}} \sum_{i=0}^{\mathcal{K}} s_{qi} d^i \sum_{j=0}^{\mathcal{K}} u_{qj} w^j \sum_{k=0}^{\mathcal{K}} v_{qk} r^k \\ &= \sum_{q=1}^{\mathcal{R}} \mathcal{H}(d; \vec{s}_q) \mathcal{H}(w; \vec{u}_q) \mathcal{H}(r; \vec{v}_q), \end{aligned} \quad (7)$$

where \mathcal{H} represents univariate polynomial. In practice, we take Eq. (7) as our MAP and control its flexibility by adjusting \mathcal{R} . A smaller \mathcal{R} indicates a simpler MAP. Empirically, we find that $\mathcal{R} = 1$ is enough for achieving an accurate regression results in most cases, which provides our MAP with a more concise form. We also show through experiments that $\mathcal{R} = 1$ makes sense because it accords with the prior of the MAP (Section 4.3).

3.2.3. FAST DATA COLLECTION

To collect data used for MAP's regression, instead of training many models with different (d, w, r) from scratch, we

³For the convenience of writing, we assume the same highest degree \mathcal{K} for d, w , and r , though conclusions in this section also hold when they have different \mathcal{K} .

⁴The definition of tensor rank is as (Bourbaki, 2003).

Algorithm 1 Iterative Pruning and Fine-tuning

Input: pre-trained M_0 , rounds rds , pruning setting T .
Initialize $data = \{(d_0, w_0, r_0, a_0)\}$,
 $d_{min} = Td_0, w_{min} = \sqrt{T}w_0, r_{min} = \sqrt{T}r_0$;
for \mathcal{A} in $\{d, w, r\}$ **do**
 for $n = 1$ **to** rds **do**
 $\mathcal{A}_n = \mathcal{A}_{n-1} - \frac{\mathcal{A}_0 - \mathcal{A}_{min}}{rds}$; ▷ \mathcal{A} means $d/w/r$
 Pruning M_{n-1} **along** \mathcal{A} -dim **to** $\mathcal{A}_n \rightarrow M_n$;
 Fine-tuning $M_n \rightarrow (d_n, w_n, r_n, a_n)$;
 Add (d_n, w_n, r_n, a_n) **to** $data$;
 end for
end for

apply iterative pruning and fine-tuning to acquire the data:

Iterative Pruning and Fine-tuning: As shown in Algorithm 1, the pre-trained model M_0 is pruned along three dimensions independently. At each dimension, we iteratively apply pruning and fine-tuning on M_0 to generate many models, and the configurations of these models (d_n, w_n, r_n, a_n) are collected for the MAP's regression. d_{min} in Algorithm 1 indicates that if we reduce the model's depth to d_{min} , the computational cost constraint T can be fulfilled without pruning the model's width and input resolution. It is easy to deduce that the optimal $d^* \geq d_{min}$. Likewise, w_{min} and r_{min} are minimal possible values for w and r , respectively.

Compared with training models from scratch, our data collection policy has two advantages: (1) A pruned pre-trained model converges faster than scratch training, thus takes less time to get a new model. (2) Besides the final pruned model, iterative pruning yields several intermediate models as well as their configurations (d_n, w_n, r_n, a_n) , which can also be used for the MAP's regression.

3.2.4. OPTIMIZING THE MAP

With the collected data, we fit the MAP by using a regression algorithm. Then, the optimal (d^*, w^*, r^*) satisfies Eq. (8) according to the Lagrange's multiplier theorem, where λ is the Lagrange multiplier.

$$\begin{cases} dw^2 r^2 - T \times d_0 w_0^2 r_0^2 = 0 \\ \sum_{q=1}^{\mathcal{R}} \mathcal{H}'(d; \vec{s}_q) \mathcal{H}(w; \vec{u}_q) \mathcal{H}(r; \vec{v}_q) + \lambda w^2 r^2 = 0 \\ \sum_{q=1}^{\mathcal{R}} \mathcal{H}(d; \vec{s}_q) \mathcal{H}'(w; \vec{u}_q) \mathcal{H}(r; \vec{v}_q) + 2\lambda dw r^2 = 0 \\ \sum_{q=1}^{\mathcal{R}} \mathcal{H}(d; \vec{s}_q) \mathcal{H}(w; \vec{u}_q) \mathcal{H}'(r; \vec{v}_q) + 2\lambda dw^2 r = 0 \end{cases} \quad (8)$$

3.3. Comprehensive Pruning and Fine-tuning

With the optimal (d^*, w^*, r^*) , filter-level pruning and layer-level pruning methods are used to prune the model to target

d^* and w^* , and then the model is fine-tuned with images of size r^* . During the pruning process, layer pruning first and filter pruning first are both viable and yield the same pruned model. Without loss of generality, we describe the process by assuming layer pruning first, and the steps are as follows:

Pruning Layers: Following DBP (Wang et al., 2019b), we put a linear classifier after each layer of model M_0 and test its accuracy on the evaluation dataset. The accuracy of each linear classifier indicates the discrimination of its corresponding layer’s features. Further, each layer’s discrimination enhancement compared with its preceding layer is seen as the importance of the layer. With this importance metric, we pick out the least important $(1 - d^*/d_0) \times 100\%$ layers and remove them from M_0 , yielding M_{p1} .

Pruning Filters: The filter-level pruning is proceeded on M_{p1} . In particular, we use the scaling factor of BN layers as the importance metric, just like Slimming (Liu et al., 2017). However, different from Slimming that compares the importance of all filters globally, we only compare the importance of filters in the same layer, and the least important $(1 - w^*/w_0) \times 100\%$ filters of each layer are pruned. With such modification, we keep all layers’ pruned ratios the same. Assume that the model after filter pruning is M_{p2} .

Fine-tuning with Smaller Images: After pruning, the pruned model M_{p2} is fine-tuned with images of size r^* . The images are resized with the bilinear down-sampling method, which is the most common downsampling for images. The model will be fine-tuned with a small learning rate till convergence, leading to the final pruned model M_p .

4. Experiments

4.1. Experimental Settings

Datasets: We take three popular datasets as testbeds of our algorithm: CIFAR-10 (Krizhevsky et al., 2009), TinyImageNet (Wu et al., 2017), and ImageNet (Russakovsky et al., 2015). These three datasets differ in their image-resolution (32×32 to 224×224), number of classes (10 to 1000), and scale of datasets (50K to 1000K images). For all datasets, images are augmented by symmetric padding, random clipping, and randomly horizontal flip, all of which are common (He et al., 2016; Howard et al., 2017; Wang et al., 2019a) augmentation methods for these datasets.

Architectures: We test our algorithm on three popular architectures: ResNet (He et al., 2016), DenseNet (Huang et al., 2017) and EfficientNet (Tan & Le, 2019). Their basic blocks vary from residual blocks to densely connected blocks and NAS-searched blocks, representing three of most popular designs for deep CNNs.

Evaluation Protocol: Following the conventions of previous works (Li et al., 2020; Lin et al., 2020; Ye et al., 2020), we take the accuracy, parameters-reduction-ratio (Prr) and FLOPs-reduction-ratio (Frr) as the evaluation protocol of our model acceleration algorithm. Prr and Frr are defined as Eq. (9), where M_0 and M_p represent the base model and the pruned model, respectively.

$$Prr = 1 - \frac{Params(M_p)}{Params(M_0)}, Frr = 1 - \frac{FLOPs(M_p)}{FLOPs(M_0)}. \quad (9)$$

Compared Algorithms: The compared algorithms fall into three categories: (1) Algorithms pruning the model along one dimension (i.e., depth, width, or resolution), including \mathcal{R} -only (Howard et al., 2017), \mathcal{W} -only (Liu et al., 2017), FPGM (He et al., 2019), DBP (Wang et al., 2019b), PScratch (Wang et al., 2020), DHP (Li et al., 2020) and HRank (Lin et al., 2020); (2) Algorithms that prune along multi-dimensions, such as GAL (Lin et al., 2019); (3) NAS-based algorithms, EfficientNet (Tan & Le, 2019) and TinyNet (Han et al., 2020), which balance the size of three dimensions from architecture search perspective.

Training Settings: For base models trained on CIFAR-10, we set the batch size to 64 for DenseNet and 128 for ResNet. Weight decay is set to 10^{-4} . The models are trained for 160 epochs with the learning rate starting from 0.1 and divided by 10 at epoch 80 and 120. These are all the most common training settings (He et al., 2016; Howard et al., 2017; Wang et al., 2019a) for models trained on CIFAR-10. For ResNet and DenseNet trained on TinyImageNet and ImageNet, the batch size is set to 256, and weight decay is 10^{-4} . Models are trained for 100 epochs. The learning rate is set to 0.1 at the beginning and multiplies 0.1 at epoch 30, 60, and 90. For EfficientNet, we apply the same training policy as (Han et al., 2020), which is also the most common for EfficientNet implemented with Pytorch (Paszke et al., 2017).

Regression and Pruning Settings: The MAP’s hyper-parameters are set to $\mathcal{R} = 1$ and $\mathcal{K} = 3$ in our pruning experiments. When collecting training data (i.e., $(d_n, w_n, r_n), n \in [1, N]$) for the polynomial regression, the model is pruned along each dimension for four times (i.e., $rds = 4$ in Algorithm 1). ResNet and DenseNet trained on CIFAR-10 are fine-tuned for 40 epochs at each round, and for 80 epochs after comprehensive pruning. Thus, the data collection process consumes as much time as training 3 models (training one model from scratch costs 160 epochs). Similarly, models trained on TinyImageNet and ImageNet are fine-tuned for 30 epochs at each round of the iterative pruning process. Therefore, it takes about the same time as training 3.6 models for the data collection process. The final pruned models trained on TinyImageNet and ImageNet are fine-tuned for 60 epochs after comprehensive pruning.

Table 1. Pruning results on CIFAR-10 and TinyImageNet. \mathcal{D} , \mathcal{W} and \mathcal{R} indicate whether the model will be pruned along depth, width, and resolution dimension, respectively. “Acc. Drop” means the accuracy loss induced by pruning (smaller is better). Results with † are drawn from original papers, and others are run with their published code with slight modifications. Our algorithm achieves **smaller accuracy losses than others with similar Prr and Frr** .

Dataset	Architecture	Algorithm	\mathcal{D}	\mathcal{W}	\mathcal{R}	Baseline	Accuracy	Acc. Drop	Prr	Frr	
CIFAR-10	ResNet-32	\mathcal{R} -only (Howard et al., 2017)			✓	93.18%	90.19%	2.99%	-	0.52	
		\mathcal{W} -only (Liu et al., 2017)		✓		93.18%	92.16%	1.02%	0.47	0.47	
		\mathcal{D} -only DBP (Wang et al., 2019b)	✓			93.18%	92.65%	0.53%	0.28	0.48	
		GAL (Lin et al., 2019)	✓	✓		93.18%	91.72%	1.46%	0.39	0.50	
		FPGM† (He et al., 2019)			✓	92.63%	92.31%	0.32%	-	0.42	
		PScratch (Wang et al., 2020)			✓	93.18%	92.18%	1.00%	-	0.50	
		Ours	✓	✓	✓	93.18%	93.27%	-0.09%	0.38	0.49	
	ResNet-56	\mathcal{R} -only (Howard et al., 2017)				✓	93.69%	92.00%	1.69%	-	0.51
		\mathcal{W} -only (Liu et al., 2017)			✓		93.69%	92.97%	0.72%	0.50	0.50
		\mathcal{D} -only DBP (Wang et al., 2019b)	✓				93.69%	93.27%	0.42%	0.40	0.52
		GAL† (Lin et al., 2019)	✓	✓			93.26%	93.38%	-0.12%	0.12	0.38
		FPGM† (He et al., 2019)			✓		93.59%	93.26%	0.33%	-	0.52
		PScratch† (Wang et al., 2020)			✓		93.23%	93.05%	0.18%	-	0.50
		HRank† (Lin et al., 2020)			✓		93.26%	93.17%	0.09%	0.42	0.50
		DHP (Li et al., 2020)			✓		93.65%	93.58%	0.07%	0.42	0.49
	Ours	✓	✓	✓		93.69%	93.76%	-0.07%	0.40	0.50	
	DenseNet-40	\mathcal{R} -only (Howard et al., 2017)				✓	94.59%	92.88%	1.71%	-	0.53
		\mathcal{W} -only (Liu et al., 2017)			✓		94.59%	94.26%	0.33%	0.65	0.65
		\mathcal{D} -only DBP (Wang et al., 2019b)	✓				94.59%	94.02%	0.57%	0.60	0.46
		GAL† (Lin et al., 2019)	✓	✓			94.81%	94.50%	0.31%	0.57	0.55
		HRank† (Lin et al., 2020)			✓		94.81%	93.68%	1.13%	0.54	0.61
		DHP† (Li et al., 2020)			✓		94.74%	93.94%	0.80%	0.36	0.62
		Ours	✓	✓	✓		94.59%	94.54%	0.05%	0.66	0.66
	ResNet-56	\mathcal{R} -only (Howard et al., 2017)				✓	56.55%	54.64%	1.91%	-	0.49
\mathcal{W} -only (Liu et al., 2017)				✓		56.55%	52.45%	4.10%	0.54	0.53	
\mathcal{D} -only DBP (Wang et al., 2019b)		✓				56.55%	55.57%	0.98%	0.25	0.53	
GAL (Lin et al., 2019)		✓	✓			56.55%	55.87%	0.68%	0.32	0.52	
DHP (Li et al., 2020)				✓		56.55%	55.82%	0.73%	0.46	0.55	
Ours		✓	✓	✓		56.55%	56.04%	0.51%	0.34	0.59	
ResNet-101		\mathcal{R} -only (Howard et al., 2017)				✓	64.83%	55.48%	9.35%	-	0.75
	\mathcal{W} -only (Liu et al., 2017)			✓		64.83%	63.47%	1.36%	0.75	0.75	
	\mathcal{D} -only DBP (Wang et al., 2019b)	✓				64.83%	61.35%	3.48%	0.76	0.77	
	GAL (Lin et al., 2019)	✓	✓			64.83%	64.33%	0.50%	0.45	0.76	
	DHP (Li et al., 2020)			✓		64.83%	64.82%	0.01%	0.50	0.75	
	Ours	✓	✓	✓		64.83%	65.27%	-0.44%	0.51	0.75	
	DenseNet-100	\mathcal{R} -only (Howard et al., 2017)				✓	61.34%	56.97%	4.37%	-	0.75
\mathcal{W} -only (Liu et al., 2017)				✓		61.34%	59.56%	1.78%	0.75	0.75	
\mathcal{D} -only DBP (Wang et al., 2019b)		✓				61.34%	58.44%	2.90%	0.65	0.78	
GAL (Lin et al., 2019)		✓	✓			61.34%	59.03%	2.31%	0.78	0.70	
DHP (Li et al., 2020)				✓		61.34%	59.40%	1.94%	0.73	0.73	
Ours		✓	✓	✓		61.34%	60.22%	1.12%	0.73	0.75	

4.2. Results and Analysis

Results on CIFAR-10 and TinyImageNet: The experimental results on CIFAR-10 and TinyImageNet are shown in Table 1. As we can see, \mathcal{W} -only induces larger loss than \mathcal{D} -only for ResNet-32 and ResNet-56, while for ResNet-101, the situation is opposite. In other words, the importance of different dimensions lies in the original size of *depth*, *width*, and *resolution*, and we cannot deduce it from simple prior, which further show the essentiality of our algorithm. We balance the size of three dimensions dynamically and always achieve better results than pruning one or two dimensions. The most competitive opponent of our algorithm is DHP — it achieves similar accuracy and Frr to our algorithm for ResNet-56 trained on both datasets. However, we show

much higher accuracy than it on DenseNet-40 for CIFAR-10 (94.54% vs. 93.94%), ResNet-101 (65.27% vs. 64.82%), and DenseNet-100 (60.22% vs. 59.40%) for TinyImageNet with similar Prr and Frr , which shows the robustness of our algorithm across different architectures and datasets.

Results on ImageNet: Experiments with ImageNet are done on ResNet-50 and DenseNet-121. As we can see in Table 2, our algorithm achieves 0.45% higher accuracy on ResNet-50 than state-of-the-art algorithms (DHP and PScratch) with the same Frr . The improvement on DenseNet-121 is marginal because compared with the model’s width, its depth and resolution are too small to prune. After comprehensive consideration, our algorithm also deems that we should mainly prune filters of DenseNet-

Table 2. Pruning Results on ImageNet. The improvement on DenseNet-121 is marginal because of DenseNet-121’s property. Detailed reasons are described in Section 4.2.

Algorithm	\mathcal{D}	\mathcal{W}	\mathcal{R}	Accuracy	Prr	Frr
ResNet-50 (76.15%)						
\mathcal{R} -only (Howard et al., 2017)		✓		71.56%	-	0.50
\mathcal{W} -only (Liu et al., 2017)		✓		74.52%	0.50	0.50
DBP (Wang et al., 2019b)	✓			73.92%	0.56	0.50
GAL [†] (Lin et al., 2019)	✓	✓		71.95%	0.17	0.43
FPGM [†] (He et al., 2019)		✓		74.83%	-	0.54
PScratch [†] (Wang et al., 2020)		✓		75.45%	0.64	0.50
HRank [†] (Wang et al., 2020)		✓		74.98%	0.37	0.44
DHP (Li et al., 2020)		✓		75.45%	0.54	0.50
Ours	✓	✓	✓	75.90%	0.53	0.50
DenseNet-121 (75.01%)						
\mathcal{R} -only (Howard et al., 2017)			✓	73.07%	-	0.51
\mathcal{W} -only (Liu et al., 2017)		✓		73.58%	0.51	0.51
DBP (Wang et al., 2019b)	✓			68.08%	0.66	0.37
Ours	✓	✓	✓	73.68%	0.48	0.51

Table 3. Comparison with NAS-based model acceleration algorithms. They all take EfficientNet-B0 as the baseline model. GPU-days is measured with NVIDIA V100. Note that training an EfficientNet from scratch costs about 8.7 GPU days.

Algorithm	Params	FLOPs	Top-1/Top-5 Acc.	Search Cost (GPU days)
EfficientNet-B0	5.3M	387M	76.7%/93.2%	-
TinyNet-A [†]	5.1M	339M	76.8%/93.3%	~ 520
Ours	5.1M	314M	76.8%/93.3%	26
EfficientNet-B ⁻¹	3.6M	201M	74.7%/92.1%	-
TinyNet-B [†]	3.7M	202M	75.0%/92.2%	~ 520
Ours	3.6M	198M	75.2%/92.7%	24
EfficientNet-B ⁻²	3.0M	98M	70.5%/89.5%	-
TinyNet-C [†]	2.5M	100M	71.2%/89.7%	~ 520
Ours	3.1M	98M	71.6%/89.9%	21

121 for acceleration. Therefore, it produces similar pruning results to filter-level pruning. However, the results do not imply our algorithm is powerless. On the contrary, **a pruning policy with a comprehensive consideration is always better than an arbitrary one, though they may produce similar results sometimes.**

Comparison with NAS-based Methods: Algorithms that balance the three dimensions (i.e., depth, width, and resolution) in a NAS manner are also compared, and results are shown in Table 3. GPU-days is the most common protocol to evaluate the search cost of NAS algorithms, which indicates natural days they spend if running with only one GPU. Both EfficientNet (Tan & Le, 2019) and TinyNet (Han et al., 2020) employ so many resources in searching the optimal (d^*, w^*, r^*) , while we do not have enough GPUs to reproduce their searching process. Thus, results of EfficientNet and TinyNet are both drawn from (Han et al., 2020), and their search cost is estimated through the number of models they train. For example, training an EfficientNet

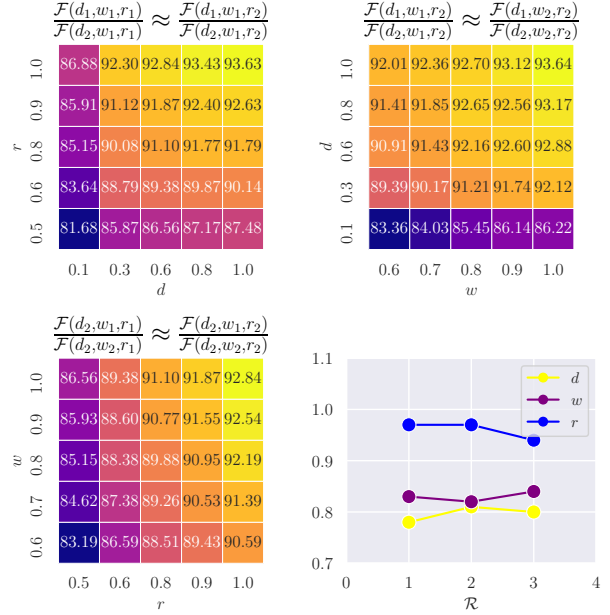


Figure 3. Accuracy of ResNet with different (d, w, r) trained on CIFAR-10 (the first three sub-figures) and the predicted optimal (d^*, w^*, r^*) with different \mathcal{R} in Eq. (10).

for 300 epochs takes about 26 hours with $8 \times V100$ GPUs, while TinyNet requires to train 60 EfficientNet models from scratch. So, its search cost is about 520 GPU days. Instead, our algorithm only spends about $\frac{1}{25}$ as much time as TinyNet for searching but achieves similar accuracy to it.

4.3. Ablation Study

Rank of Λ : In Section 3.2.2, our proposed MAP is:

$$\mathcal{F}(d, w, r; \Lambda) = \sum_{q=1}^{\mathcal{R}} \mathcal{H}(d; \vec{s}_q) \mathcal{H}(w; \vec{u}_q) \mathcal{H}(r; \vec{v}_q), \quad (10)$$

where the rank of Λ is less than or equal to \mathcal{R} . Experimentally, we find that $\mathcal{R} = 1$ works well in most cases. To further explore this interesting phenomenon, ResNet with different (d, w, r) are trained on CIFAR-10. The base model (i.e., $(d, w, r) = (1.0, 1.0, 1.0)$) is ResNet-32 with images of size 32, and results are shown in Figure 3. Observations from the first three sub-figures are shown in their titles. We can deduce from these observations⁵:

$$\mathcal{F}(d, w, r; \Lambda) \approx \mathcal{H}(d; \vec{s}_q) \mathcal{H}(w; \vec{u}_q) \mathcal{H}(r; \vec{v}_q), \quad (11)$$

which coincides with Eq. (10) when $\mathcal{R} = 1$. In other words, three variables (d, w, r) in the MAP can be approximately separated from each other. We also test the MAP with different \mathcal{R} , as shown in the 4th sub-figure of Figure 3. The MAP with larger \mathcal{R} yields similar (d^*, w^*, r^*) to that of

⁵More results and the proof are put in our supplementary materials.

Table 4. MAP’s regression results with lower degree or regularization. \mathcal{K} means the highest degree for each variable in (d, w, r) . l_2 is the coefficient of the regularization term, and 0 indicates no regularization.

Type	\mathcal{K}	l_2	Train Err.	Eval Err.
Normal Polynomial	1	0	2.66%	2.97%
	2	0	1.62%	2.25%
	3	0	0.28%	1.28%
	5	0	0.02%	2.31%
	5	10^{-3}	0.02%	2.28%
	10	0	0.01%	2.58%
	10	10^{-3}	0.02%	2.32%
Ours	3	0	0.14%	0.33%
	5	0	0.08%	0.25%

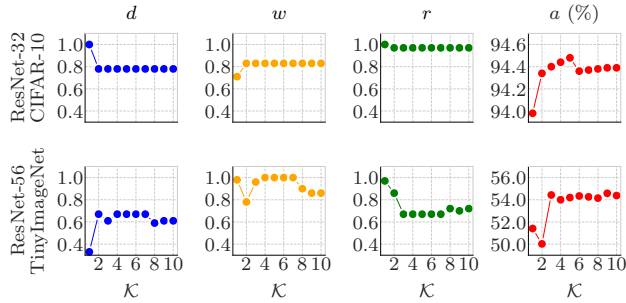


Figure 4. Predicted optimal (d^*, w^*, r^*) and corresponding pruning results with different \mathcal{K} . For all $\mathcal{K} \geq 3$, the MAP’s predicted optimal (d^*, w^*, r^*) are very similar. Users do not need to bother to choose \mathcal{K} carefully.

$\mathcal{R} = 1$, which also indicates that $\mathcal{R} = 1$ is enough for a well-performed MAP.

Other Methods of Avoiding Overfitting: Besides restricting the rank of Λ , we also try another two methods of avoiding overfitting, i.e., decreasing the degree (\mathcal{K}) of polynomials and applying regression with regularization terms. The results are in Table 4. Specifically, 13 sets of (d_n, w_n, r_n, a_n) are used to fit the MAP, and other 80 sets of (d_n, w_n, r_n, a_n) are used for evaluation. All data is collected with ResNet-56 trained on CIFAR-10. Training error and evaluation error are both reported. As we can see, normal polynomial regression induces severe overfitting and high evaluation loss, and l_2 -regularization is also limited in solving the overfitting issue. Still, lowering the degree of polynomials is not a wise choice because it makes the polynomial fail to converge even on training data. Instead, our specialized MAP shows a lower error rate on both training data (0.08%) and evaluation data (0.25%).

Influence of Polynomials’ Degree: Figure 4 shows the pruning results when adjusting the MAP’s degree \mathcal{K} . Especially, the polynomial regression degrades to linear regression when $\mathcal{K} = 1$. As we can see, for polynomials with $\mathcal{K} \leq 2$, the predicted optimal (d^*, w^*, r^*) actually leads to

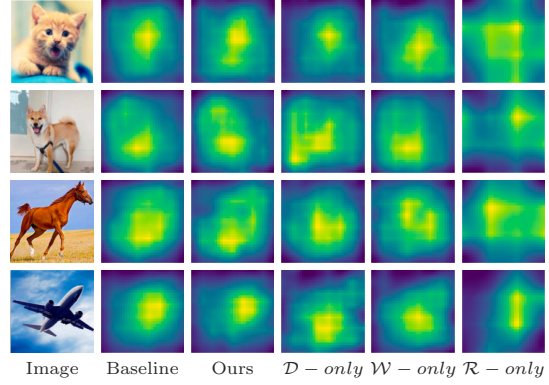


Figure 5. Visualizations of last layer’s feature maps from different models. The baseline model is a pre-trained ResNet-56. Four different pruning policies are tested, and our pruned model’s feature maps look most like those of baseline models.

a sub-optimal pruning policy, which indicates that the MAP is too simple to use. For polynomials with $\mathcal{K} \geq 3$, all MAPs generate similar predictions about the optimal (d, w, r) , i.e., $(0.78, 0.82, 0.98)$ for ResNet-32 trained on CIFAR-10 and $(0.65, 1.0, 0.63)$ for ResNet-56 trained on TinyImageNet. The results indicate that our algorithm is relatively robust to different degrees \mathcal{K} , and practitioners are disengaged from choosing the polynomial degree carefully.

4.4. Case Study

Visualization of Feature Maps for Different Pruning Policies: In order to further understand why pruning three dimensions simultaneously yields better results than pruning one, Figure 5 compares the feature maps for models with different pruning policies. Specifically, all models are pruned from the same baseline model — a ResNet-56 pre-trained on CIFAR-10. Input images are randomly chosen from the internet. For visualization, we extract the last convolutional layer’s feature maps and compute their mean absolute values across channels. As we can see, the feature maps that our pruned model outputs look most similar to those of the original model. This indicates that we preserve most information of the original model by pruning three dimensions comprehensively.

5. Conclusion

We proposed a pruning framework that prunes three dimensions comprehensively. It first determines the optimal (d^*, w^*, r^*) by optimizing our specialized MAP and prunes models in terms of (d^*, w^*, r^*) . The results show that our algorithm outperforms SOTA pruning algorithms with similar computational cost by pruning three dimensions comprehensively. Compared with NAS-based methods, we generated pruned models slightly outperforming theirs with much less search cost. In the future, we will generalize our approach to other vision tasks like object detection, segmentation, etc.

References

- Ba, J. and Caruana, R. Do deep nets really need to be deep? In *NeurIPS*, 2014.
- Bishop, C. M. *Pattern Recognition and Machine Learning*. Springer, 2006.
- Bourbaki, N. *Elements of mathematics: Algebra*. Springer, 2003.
- Frankle, J. and Carbin, M. The lottery ticket hypothesis: Finding sparse, trainable neural networks. In *ICLR*, 2019.
- Han, K., Wang, Y., Zhang, Q., Zhang, W., Xu, C., and Zhang, T. Model rubik’s cube: Twisting resolution, depth and width for tinynets. *NeurIPS*, 2020.
- Han, S., Mao, H., and Dally, W. J. Deep compression: Compressing deep neural network with pruning, trained quantization and huffman coding. In *ICLR*, 2016.
- He, K., Zhang, X., Ren, S., and Sun, J. Deep residual learning for image recognition. In *CVPR*, 2016.
- He, Y., Kang, G., Dong, X., Fu, Y., and Yang, Y. Soft filter pruning for accelerating deep convolutional neural networks. In *IJCAI*, 2018.
- He, Y., Liu, P., Wang, Z., Hu, Z., and Yang, Y. Filter pruning via geometric median for deep convolutional neural networks acceleration. In *CVPR*, 2019.
- Hinton, G. E., Vinyals, O., and Dean, J. Distilling the knowledge in a neural network. *CoRR*, abs/1503.02531, 2015.
- Howard, A. G., Zhu, M., Chen, B., Kalenichenko, D., Wang, W., Weyand, T., Andreetto, M., and Adam, H. Mobilenets: Efficient convolutional neural networks for mobile vision applications. *CoRR*, abs/1704.04861, 2017.
- Huang, G., Liu, Z., van der Maaten, L., and Weinberger, K. Q. Densely connected convolutional networks. In *CVPR*, 2017.
- Kang, M. and Han, B. Operation-aware soft channel pruning using differentiable masks. In *ICML*, 2020.
- Kolda, T. G. and Bader, B. W. Tensor decompositions and applications. *Society for Industrial and Applied Mathematics Review*, 2009.
- Krizhevsky, A., Hinton, G., et al. Learning multiple layers of features from tiny images. Technical report, Citeseer, 2009.
- Li, H., Kadav, A., Durdanovic, I., Samet, H., and Graf, H. P. Pruning filters for efficient convnets. In *ICLR*, 2017.
- Li, Y., Gu, S., Zhang, K., Gool, L. V., and Timofte, R. DHP: differentiable meta pruning via hypernetworks. In *ECCV*, 2020.
- Lin, M., Ji, R., Wang, Y., Zhang, Y., Zhang, B., Tian, Y., and Shao, L. Hrank: Filter pruning using high-rank feature map. In *CVPR*, 2020.
- Lin, S., Ji, R., Yan, C., Zhang, B., Cao, L., Ye, Q., Huang, F., and Doermann, D. S. Towards optimal structured CNN pruning via generative adversarial learning. In *CVPR*, 2019.
- Liu, Z., Li, J., Shen, Z., Huang, G., Yan, S., and Zhang, C. Learning efficient convolutional networks through network slimming. In *ICCV*, 2017.
- Luo, J., Zhang, H., Zhou, H., Xie, C., Wu, J., and Lin, W. Thinet: Pruning CNN filters for a thinner net. *TPAMI*, 2019.
- Molchanov, P., Tyree, S., Karras, T., Aila, T., and Kautz, J. Pruning convolutional neural networks for resource efficient inference. In *ICLR*, 2017.
- Paszke, A., Gross, S., Chintala, S., Chanan, G., Yang, E., DeVito, Z., Lin, Z., Desmaison, A., Antiga, L., and Lerer, A. Automatic differentiation in pytorch. 2017.
- Russakovsky, O., Deng, J., Su, H., Krause, J., Satheesh, S., Ma, S., Huang, Z., Karpathy, A., Khosla, A., Bernstein, M. S., Berg, A. C., and Li, F. Imagenet large scale visual recognition challenge. *IJCV*, 2015.
- Simonyan, K. and Zisserman, A. Very deep convolutional networks for large-scale image recognition. In Bengio, Y. and LeCun, Y. (eds.), *ICLR*, 2015.
- Tan, M. and Le, Q. V. Efficientnet: Rethinking model scaling for convolutional neural networks. In *ICML*, 2019.
- Wang, W., Fu, C., Guo, J., Cai, D., and He, X. COP: customized deep model compression via regularized correlation-based filter-level pruning. In *IJCAI*, 2019a.
- Wang, W., Zhao, S., Chen, M., Hu, J., Cai, D., and Liu, H. DBP: discrimination based block-level pruning for deep model acceleration. *CoRR*, abs/1912.10178, 2019b.
- Wang, Y., Zhang, X., Xie, L., Zhou, J., Su, H., Zhang, B., and Hu, X. Pruning from scratch. In *AAAI*, 2020.
- Wen, W., Wu, C., Wang, Y., Chen, Y., and Li, H. Learning structured sparsity in deep neural networks. In *NIPS*, 2016.
- Wu, J., Zhang, Q., and Xu, G. Tiny imagenet visual recognition challenge. Technical report, 2017.

Ye, M., Gong, C., Nie, L., Zhou, D., Klivans, A., and Liu, Q. Good subnetworks provably exist: Pruning via greedy forward selection. In *ICML*, 2020.

A. Why the Rank of Λ Is 1

A.1. Experiments

In our original paper, we propose a model accuracy predictor (MAP):

$$\mathcal{F}(d, w, r; \Lambda) = \sum_{q=1}^{\mathcal{R}} \mathcal{H}(d; \vec{s}_q) \mathcal{H}(w; \vec{u}_q) \mathcal{H}(r; \vec{v}_q), \quad (12)$$

where \mathcal{H} represents a univariate polynomial, and \mathcal{R} means the rank of Λ . Pruning experiments shown in our original paper are done with $\mathcal{R} = 1$ because we find that $\mathcal{R} = 1$ is enough for an accurate approximation of MAP. In this case, Eq. 12 becomes:

$$\mathcal{F}(d, w, r; \Lambda) = \mathcal{H}(d; \vec{s}) \mathcal{H}(w; \vec{u}) \mathcal{H}(r; \vec{v}). \quad (13)$$

We assume that $\mathcal{R} = 1$ works well because it accords with the real distribution of $\mathcal{F}(d, w, r)$. To further identify the assumption, we design some experiments to show the relations between the model's accuracy and (d, w, r) . Specifically, we train many ResNets and DenseNets with different (d, w, r) , and results are in Table 5 — part of them are also shown in the original paper. The observations are shown in their subtitles, from which we can draw the same conclusion as Eq. 13.

A.2. Proof

Omitting all subscripts of d_1 , w_1 , and r_1 of equations in Table 5, we have:

$$\begin{aligned} \frac{\mathcal{F}(d_2, w, r)}{\mathcal{F}(d_2, w_2, r)} &\approx \frac{\mathcal{F}(d_2, w, r_2)}{\mathcal{F}(d_2, w_2, r_2)} \\ \Rightarrow \mathcal{F}(d_2, w, r) &\approx \frac{\mathcal{F}(d_2, w_2, r) \mathcal{F}(d_2, w, r_2)}{\mathcal{F}(d_2, w_2, r_2)}, \end{aligned} \quad (14)$$

$$\begin{aligned} \frac{\mathcal{F}(d, w, r)}{\mathcal{F}(d_2, w, r)} &\approx \frac{\mathcal{F}(d, w, r_2)}{\mathcal{F}(d_2, w, r_2)} \\ \Rightarrow \mathcal{F}(d, w, r) &\approx \frac{\mathcal{F}(d_2, w, r) \mathcal{F}(d, w, r_2)}{\mathcal{F}(d_2, w, r_2)}, \end{aligned} \quad (15)$$

$$\begin{aligned} \frac{\mathcal{F}(d, w, r_2)}{\mathcal{F}(d_2, w, r_2)} &= \frac{\mathcal{F}(d, w_2, r_2)}{\mathcal{F}(d_2, w_2, r_2)} \\ \Rightarrow \mathcal{F}(d, w, r_2) &= \frac{\mathcal{F}(d_2, w, r_2) \mathcal{F}(d, w_2, r_2)}{\mathcal{F}(d_2, w_2, r_2)}. \end{aligned} \quad (16)$$

Bringing Eq. 14 and Eq. 16 into Eq. 15, we have:

$$\begin{aligned} \mathcal{F}(d, w, r) &\approx \frac{\mathcal{F}(d, w_2, r_2) \mathcal{F}(d_2, w, r_2) \mathcal{F}(d_2, w_2, r)}{\mathcal{F}(d_2, w_2, r_2)^2} \\ &= \frac{\mathcal{H}(d; \vec{s}) \mathcal{H}(w; \vec{u}) \mathcal{H}(r; \vec{v})}{\mathcal{F}(d_2, w_2, r_2)^2}, \end{aligned} \quad (17)$$

where $\frac{1}{\mathcal{F}(d_2, w_2, r_2)^2}$ is a constant and can be merged into any \mathcal{H} . Thus, Eq. 17 can be re-formulated as:

$$\mathcal{F}(d, w, r) \approx \mathcal{H}(d; \vec{s}) \mathcal{H}(w; \vec{u}) \mathcal{H}(r; \vec{v}), \quad (18)$$

which complies with Eq. 13.

Table 5. Accuracy (%) of ResNets and DenseNets on CIFAR-10 with different width (w) and resolution (r). The base models are ResNet-32 and DenseNet-40.

(a) $\frac{\mathcal{F}(d_2, w_1, r_1)}{\mathcal{F}(d_2, w_2, r_1)} \approx \frac{\mathcal{F}(d_2, w_1, r_2)}{\mathcal{F}(d_2, w_2, r_2)}$						(b) $\frac{\mathcal{F}(d_1, w_1, r_1)}{\mathcal{F}(d_2, w_1, r_1)} \approx \frac{\mathcal{F}(d_1, w_1, r_2)}{\mathcal{F}(d_2, w_1, r_2)}$						(c) $\frac{\mathcal{F}(d_1, w_1, r_2)}{\mathcal{F}(d_2, w_1, r_2)} \approx \frac{\mathcal{F}(d_1, w_2, r_2)}{\mathcal{F}(d_2, w_2, r_2)}$					
ResNet ($d = 1.0$)						ResNet ($w = 1.0$)						ResNet ($r = 1.0$)					
$w \backslash r$	1.00	0.87	0.75	0.62	0.50	$d \backslash r$	1.00	0.87	0.75	0.62	0.50	$w \backslash d$	0.11	0.33	0.55	0.77	1.00
0.60	90.59	89.43	88.51	86.59	83.19	0.11	86.88	85.91	85.15	83.64	81.68	0.60	83.36	89.39	90.91	91.41	92.01
0.70	91.39	90.53	89.26	87.38	84.62	0.33	92.30	91.12	90.08	88.79	85.87	0.70	84.03	90.17	91.43	91.85	92.36
0.80	92.19	90.95	89.88	88.38	85.15	0.55	92.84	91.87	91.10	89.38	86.56	0.80	85.45	91.21	92.16	92.65	92.7
0.90	92.54	91.55	90.77	88.60	85.93	0.77	93.43	92.40	91.77	89.87	87.17	0.90	86.14	91.74	92.60	92.56	93.12
1.00	92.84	91.87	91.10	89.38	86.56	1.00	93.63	92.63	91.79	90.14	87.48	1.00	86.22	92.12	92.88	93.17	93.64
DenseNet ($d = 1.0$)						DenseNet ($w = 1.0$)						DenseNet ($r = 1.0$)					
$w \backslash r$	1.00	0.87	0.75	0.62	0.50	$d \backslash r$	1.00	0.87	0.75	0.62	0.50	$w \backslash d$	0.20	0.40	0.60	0.80	1.00
0.60	90.82	90.48	89.62	88.04	85.63	0.20	88.16	87.64	86.77	85.50	83.83	0.60	84.51	88.82	89.95	91.40	92.70
0.70	91.54	90.98	90.19	88.79	86.75	0.40	92.00	91.22	90.32	89.15	86.89	0.70	85.43	89.26	90.51	92.35	92.83
0.80	91.99	91.57	90.59	90.01	87.67	0.60	93.03	92.06	91.85	90.63	88.42	0.80	86.92	90.75	91.07	93.01	93.66
0.90	92.74	92.08	91.19	90.56	88.12	0.80	93.80	93.21	92.78	91.74	89.25	0.90	87.88	91.74	91.46	93.14	93.86
1.00	93.09	92.25	92.05	90.68	88.38	1.00	94.53	93.75	93.69	92.21	89.84	1.00	88.16	92.00	93.03	93.80	94.53